

Journal of Materials Chemistry A

Accepted Manuscript



This is an *Accepted Manuscript*, which has been through the Royal Society of Chemistry peer review process and has been accepted for publication.

Accepted Manuscripts are published online shortly after acceptance, before technical editing, formatting and proof reading. Using this free service, authors can make their results available to the community, in citable form, before we publish the edited article. We will replace this *Accepted Manuscript* with the edited and formatted *Advance Article* as soon as it is available.

You can find more information about *Accepted Manuscripts* in the [Information for Authors](#).

Please note that technical editing may introduce minor changes to the text and/or graphics, which may alter content. The journal's standard [Terms & Conditions](#) and the [Ethical guidelines](#) still apply. In no event shall the Royal Society of Chemistry be held responsible for any errors or omissions in this *Accepted Manuscript* or any consequences arising from the use of any information it contains.

ARTICLE

Full capacitance potential of SWCNT electrode in ionic liquids at 4V

Cite this: DOI: 10.1039/x0xx00000x

Yuntao Yu, Chaojie Cui, Weizhong Qian*, Fei Wei

Received 00th January 2012,

Accepted 00th January 2012

DOI: 10.1039/x0xx00000x

www.rsc.org/

We studied the full capacitance potential of single walled carbon nanotube (SWCNT, 1250 m²/g) in EMIBF₄ at 4V by a new charge mode with certain dwelling time at 4 V. This allowed the accessible surface area of SWCNT, in monodispersed state and with macropores in large amount, was fully explored to exhibit capacitance of 16 μF/cm² in wide range of current density, higher than that (9.1 μF/cm²) of a graphene (5 μm in size and 2200 m²/g). *In situ* Raman characterization upon charge and discharge validated the enhanced doping of ions of EMIBF₄ on SWCNT wall with the increased potential. The energy density is 107 Wh/kg at power density of 20 kW/kg, far exceeding that (64 Wh/kg) in conventional galvanostatic charge and discharge mode.

Introduction

Supercapacitor (SC) received much attention recently, owing to the increasing importance of clean electrochemical energy storage for sustainable development of human society.^{1a,1b} The development of high voltage SC with high energy density, mainly depending on the carbon-based electrode, is crucial to the commercial application in electrical vehicles and other heavy apparatus calling for high power density.^{1c-1f,2a} Capacities of energy storage and energy release of these electrodes, including carbon nanotube (CNT) and graphene, directly depends on their accessible specific surface area (SSA) and structural configuration to provide electrode/electrolyte interface upon charge and relatively short diffusion distance of ions of electrolyte.² Specifically, single walled CNT (SWCNT) or single layer graphene, as in the monodispersed state, had high surface area and dominated exohedral surface and would be the ideal platform for the deposition of ions of electrolyte upon charge.^{1c,2c,2d,2f} But the practical capacitance of SWCNT electrode is only 13-15 μF/cm² in 4V electrolytes such as organic electrolyte or ionic liquids (ILs),^{1a,2a} lower than that (about 21 μF/cm²) of theoretical value of graphene.^{2b} And the capacitance or energy density of electrode decreased drastically with the increase of the power density. It remained unknown that it is electrode structural limited or charge mode limited to this date. Understanding the full potential of SWCNT electrode in storing energy, as well as elevating its energy density in high power density is not only highly desirable in practical application, but also very useful for the development of other high performance electrodes in the future.

In order to address this issue, we used a charge mode with dwelling time at certain voltage to study the full capacitance potential of SWCNT electrode, rather than the use of galvanostatic charge and discharge mode. Although the former charge mode was already used in SC industry, but is firstly used in the system of using ILs electrolyte and operated at 4V. In

general, SWCNT with SSA of 1250 m²/g and purity of 99% was grinded with ILs electrolyte (EMIBF₄) to achieve a nearly mono-dispersed state. Controlling the weight ratio of SWCNT to 7% in ILs produced a very sticky gel, which was pasted on the current collector of Ni-foam. In this case, all external surface of SWCNT was completely exposed to ion of ILs. In addition, the Debye ionic screening length of ILs is nearly zero, which was most favourable for the measurement, compared to the solvated ions in organic electrolytes.^{2b} For the first time, the dischargeable capacitance of SWCNT approached to 16 μF/cm² and was independently of power density from 1 to 20 kW/kg. In comparison, a graphene (size: 5 μm, SSA: 2200 m²/g, Fig.1b, 1d) was unable to be charged successfully to achieve such high value and only had a capacitance of 9.4 μF/cm², due to the limitation of long ion diffusion distance and the lack of macropores in large amount. *In situ* Raman characterization validated the enhanced doping of ions of electrolyte on tube with the increase of the applied potential.⁴ The dischargeable energy density is 107 Wh/kg at the power density of 20 kW/kg, 67% higher than that (64 Wh/kg) in conventional galvanostatic charge and discharge mode. The result highlighted SWCNT as a promising electrode for SCs in the special application calling for high energy density under high power density.

Experimental

Preparation of SWCNT or graphene electrode material

Electrode of SWCNT used here is prepared by a chemical vapor deposition method,^{3a} where methane was decomposed over Fe/Mo/MgO catalyst. The product (mixture of SWCNT and catalyst) was washed by HCl (1 mol/L, 25°C) to remove MgO support and Fe impurities. The wet SWCNT sample was freeze dried at -25 °C and 10⁻² Pa to become a loosely packed architecture with high porosity up to 97%. Further SWCNT was calcinated by CO₂ etching at, followed with HCl washing and

drying.^{3b} Brunauer–Emmett–Teller (BET) surface area of SWCNTs was recorded in a Quantachrome automated surface area and porosity analyzer with N₂ as the adsorption gas, which was 1250 m²/g (Fig.1c) and purity of 99% characterized by thermo-gravimetric analysis (TGA, TA2000, elevating heat rate of 15 °C/min, SI-1 Fig.S1).

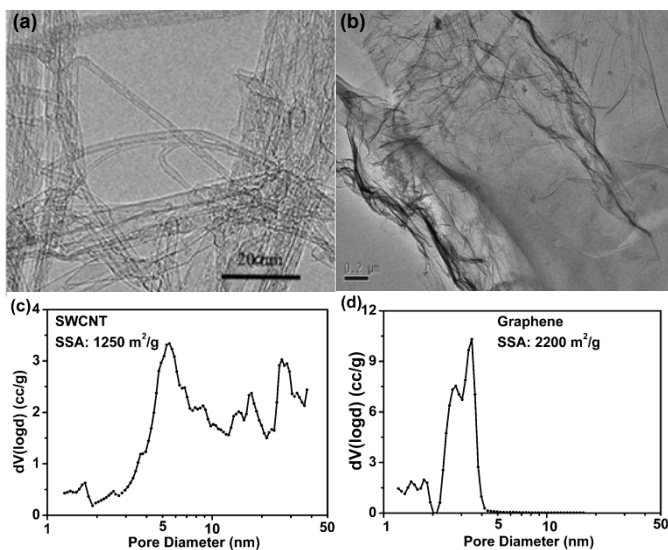


Fig.1 TEM image of (a) SWCNT and (b) graphene sample; pore size distribution of (c) SWCNT and (d) graphene sample.

Graphene sample with size of 5 μm (Fig.1b) was prepared by a modified chemical exfoliation method.^{3c} It was further treated by KOH, following the method in ref.3d, to give a product with BET surface area of 2200 m²/g (SI-1, Fig.S1). The TGA purity is about 99.5%. Oxygen of graphene is tried to be removed by H₂ etching at 900 °C for 2 hrs. The oxygen content determined by XPS is about 5%.

Fabrication of SC and capacitance performance test

SWCNT or graphene above was mixed with ionic liquids of EMIBF₄ with the weight ratio of 7:93 to make a gel in glove box with oxygen concentration of 0.3 ppm and H₂O concentration of 0.3 ppm. The sticky gel was putted on the Ni-foam current collector. The mass of activated material is 3.5 mg on each electrode sheet. Whatman membrane with thickness of 680 μm, made of glass microfiber (type: GF/D1823-047), was placed between two sheets. Finally, electrode sheets and membrane were compressed together and sealed in a coin cell with diameter of 13 mm. It is a two-electrode SC cell.

The electrochemical performance was tested by conventional galvanostatic charge and discharge mode or by a new charge mode. In latter mode, the SC cell was firstly charged at constant current from 0V to 2V or 3V or 4V. When the potential approached to the desired value (2, 3 or 4V), the cell was continuously charged and dwelled for certain times, waiting the current decreased to nearly zero. Finally the cell was discharged from 2V (or 3V, 4V) to 0V. Electrochemical impedance spectroscopy (EIS) of CNT-based SC was characterized by using a Solartron 1470E electrochemical station equipped with a 1455AFRA module. The specific capacitance under different

scan rate of 0.5-10A/g between 0-4 V was calculated based on the mass of activated material.

In situ Raman characterization

Raman spectra were characterized by a JY Horiba Raman (Aramis) under 633 nm laser for the accumulation intensity of 3 times scan. SC cell with transparent shell (Fig.2a, 3 mm in thickness) was placed under the laser. The wires were connected with electrochemical station (Fig. 2c), allowing the record of Raman signal and electrical signal simultaneously (Fig.2b). In detail, when the new charge mode was used to charge the cell, we recorded the Raman spectrum of electrode waiting the current at constant voltage decreased to nearly zero. We found it is easy to achieve a stable charge state under 0 V to 2.5 V for positively charge on BF₄⁻, and under 0 V to -2.5 V for negatively charge on EMI⁺. But it is difficult to achieve a stable charge state at 4 V, since Raman response is quite slower than the charge response.

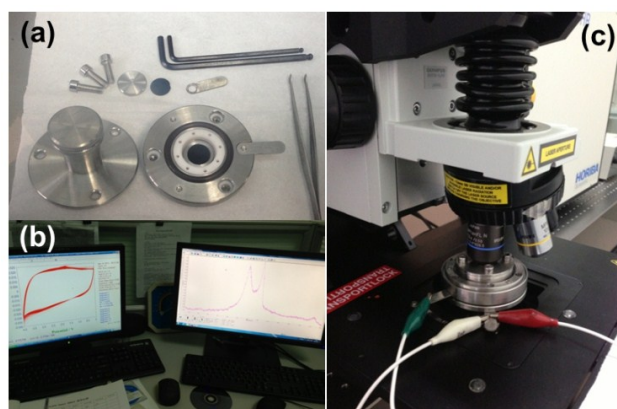


Fig.2 Photos of (a) visible SC cell components; (b) The Raman signal and electrical signal recorded simultaneously; (c) *In situ* Raman apparatus.

Results and discussion

The EIS curve of SWCNT-based SC showed in Fig.3a indicated that the tail is nearly vertical, suggesting the SC performed as a pure double layer capacitance (DLBC). The electrolyte resistance is only 1.1 Ω, and the real impedance at 1k frequency is 1.6 Ω, confirming the excellent electrical conductivity of SWCNT and well ionic conductivity of EMIBF₄. CV curve was recorded at 50 mV/s or 500 mV/s to give a regular trapezoid shape (Fig.3b). Redox reaction contributed to the faradic capacitances is insignificant, except a very small peak at 1.8 V, probably due to the presence of some Fe residue in SWCNTs (520 mg/kg Fe in sample by ICP analysis).^{1g,3b,3e} These are the basis for the study of the full potential of DLBC in the present work. As follows, we presented the charge and discharge curves in different modes. In galvanostatic charge and discharge mode, SC cell was discharged soon after the voltage approached to the desirable value (e.g. 2V in Fig.3c, 3V in Fig.3e, or 4V in Fig.3g, respectively), widely used in fundamental study to evaluate the performance of electrode. In contrast, the charge mode with dwelling time at certain voltage was widely adopted in industry and called here as new charge mode for comparison convenience. The difference from the galvanostatic charge and discharge curve lies in that there had a platform between charge

and discharge line, e.g. showed in Fig.3d, 3f and 3h at 2,3,4V, respectively. Charge time from 0V to desired value in different charge modes varied with the current density (Fig.3). And the dwelling time at 2V, 3V or 4V, till the current to nearly zero, is also different in new charge mode, because of the different charge resistances (Fig.3d, 3f, and 3h). Quantitatively, it took 442 s when charging from 0V to 4V at 0.5A/g. And 180 s was dwelled at 4V to achieve the adsorption-desorption equilibrium (Fig.3h). After that, the discharge time is 388 s at 0.5A/g. The current decay quickly in dwelling period, suggesting no much heat was produced in the new charge mode (SI-2, Fig.S2).

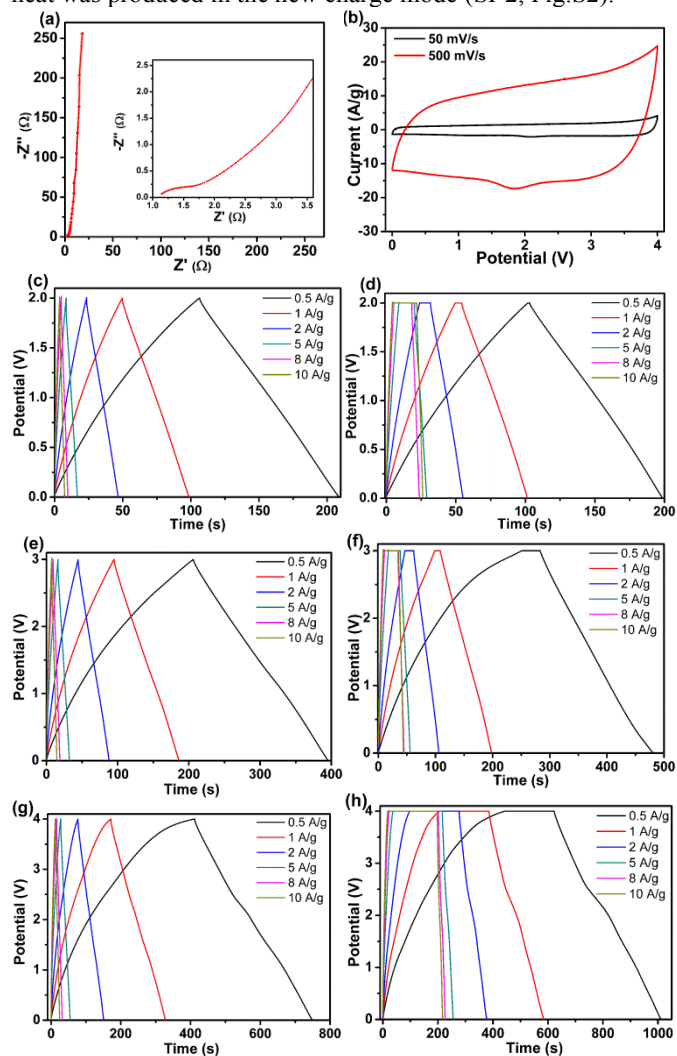


Fig.3 (a) EIS curve of SWCNT electrode; (b) CV curve of SWCNT electrode at different scanning rates; Different charge mode of SWCNT SCs: Galvanostatic charge and discharge curve at 2V(c), 3V(e), 4V(g); New charge mode with dwelling time, where SCs was firstly charged at constant current to 2V(d), 3V(f), 4V(h), then charged at constant voltage until the current is very closing to zero.

Quantitatively, the capacitance at 2V and 3V (Fig.4a), calculated by the discharge line in new charge mode, is about 100 F/g and 130 F/g, respectively. These values did not decrease with the current density (Fig.4a). Strikingly, the capacitance is 200 F/g at 4V or 16 $\mu\text{F}/\text{cm}^2$ based on its SSA (Fig.4a). We proposed that the ion doped on outer wall of tube

contributed dominantly to the capacitance, since the ions encapsulated inside the channel of tube exhibited high melting point⁵ and had low mobility unfavorable for the charge and discharge. In addition, the capacitance in new charge mode, is always equal to that in conventional charge mode at low current density (< 4A/g) and larger than the latter at high current density (4-10A/g). Moreover, with the increase of applied potential, the gap between the capacitances in different charge modes was enlarged to some degree (Fig.4a). The dischargeable capacitance in new charge mode at 4V is 203 F/g, far higher than that (130 F/g) in conventional charge mode and that in organic electrolyte (160 F/g, with an optimized electrode structure)^{1h} at 10 kW/kg (SI-3, Fig.S4). Note that the energy density of SWCNT electrode increased with the cube of voltage in previous work^{1h}, due to enhanced doping effect of ions in higher density on the tube surface (SI-3, Fig.S4). However, such effect is SWCNT structure dependent, not always correct for other carbon electrodes such as activated carbon.^{1a} Quantitatively, the energy density is 107 Wh/kg in power density of 20 kW/kg in new mode at 4V (Fig.4b), 67% higher than that (64Wh/kg) in conventional charge mode. As mentioned above, the current, after the potential was constant at 4V, decayed quickly with time (SI-2, Fig.S2). Thus, the new charge mode is repeatable (Fig.3h) and offered a special application case calling for high energy density in high power density. Moreover, when the charge and discharge mode of SC was recovered to the galvanostatic one after working under new charge mode for certain times, it still exhibited long cycling stability.

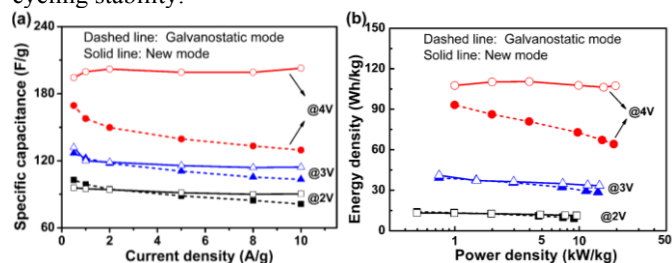


Fig.4 (a)Capacitances at different current densities (2V,3V, 4V) ; (b) Range Plot of energy density and power density.

On the other hand, we found the dwelling times were similar under different current densities to maintain the 4V platform (Fig.3h). It suggested that energy, which is unable to be charged in conventional charge mode, due to the ion-diffusion limited in high current density, can be charged in the new charge mode. As a result, the new charge mode offered SCs a new working mode independently of the current density or power density. For comparison, the capacitance performance of graphene (Fig.1b) was tested by the use of two charge modes (Fig.6a, 6b). The capacitance based on its SSA value is only 9.1 $\mu\text{F}/\text{cm}^2$ at 4V (SI-2, Fig.S3). The easy stacking of graphene with large size,^{2a,8} and the lack of macropores for the diffusion of ions (Fig.1d) resulted in the low surface efficiency. The comparison confirmed that the high capacitance performance is electrode structure dependent.^{2c} SWCNT advantaged over graphene in small diameter, dominant exohedral surface and macropores in large amount (Fig.1c), offering the average short diffusion distance and allowing the quick access of ions to its external surface when it is in the monodispersed state. In addition, we also compared the electrolyte effect on the performance of tube on high voltage. Previous work reported the similar enhanced interaction of ions in organic electrolyte with the increased potential.^{1h,2e,4a}

However, the capacitance of SWCNT is only 160 F/g at 4V in organic electrolyte, far lower than that in present work. Although many work suggested the de-solvation effect of ions in organic electrolyte whether in pores of activation carbon or SWCNT,^{7,2e} which, however, influenced the reorganization rate of ions on the electrode surface upon high potential in high current density. In addition, the large size of solvated ions, having larger diffusion resistance at 4V maybe also contributed to the lower capacitance in organic electrolyte,^{1h} compared to that of ions of pure ILs in the present work (SI-3, Fig.S4).

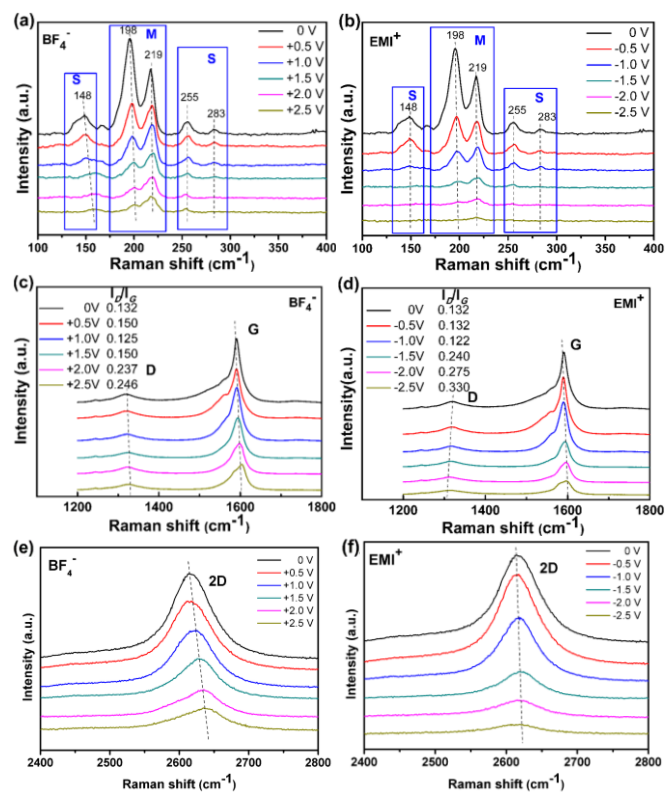


Fig.5 *In situ* Raman characterization of SWCNT in SC cell under different voltages (Raman laser is 633 nm). (a) RBM response (positive charge from 0-2.5V made the BF_4^- ion move); (b) RBM response (negative charge made the EMI^+ ion move); (c) D band and G band change (positive charge from 0-2.5V made the BF_4^- ion move); (d) D band and G band change (negative charge made the EMI^+ ion move); (e) 2D band change (positive charge from 0-2.5V made the BF_4^- ion move); (f) 2D band change (negative charge made the EMI^+ ion move).

Further, *in situ* Raman characterization was used to characterize the interaction of ILs with SWCNT or graphene, considering Raman is sensitive to the diameter change or defect band change of SWCNT or graphene as deposited on other media.⁴ SWCNT electrode in SC cell with a transparent quartz shell was detected by Raman spectroscopy upon charging (Fig.2). Note here that Raman response is rather slower than the electrical charge, therefore, it is very difficult to obtain the stable Raman information charged at 4V. Even though, we tried to elevate the potential to 2.5V, rather than 1.5 V in previous work,^{4a} to obtain information much close to that in 4V. Generally, the cell was charged positively to ensure the doping of BF_4^- on tube wall (Fig.5a,5c, 5e), or negatively charged to make the doping of EMI^+ on tube wall (Fig.5b,5d, 5f). Radial

breathing mode (RBM) of SWCNT had intensive response at 100-300 cm^{-1} and the tubes were classified into metallic tube and semiconducting tube.^{4c} The peak intensity of two metallic tubes (centered at 198 cm^{-1} , 219 cm^{-1}) decreased drastically with the increased potential. However, the peak intensity of semiconducting tubes (centered at 255 cm^{-1} , 283 cm^{-1}) is nearly unchanged. Similar, the peak positions of semiconducting tubes above are less influenced rather than those of metallic tubes above. Apparently, charge under high voltage enhanced the doping of ion on metallic SWCNT significantly. Since Raman response is sensitive to the tube diameter, the results above indicated the strong interaction of ions with tube and the reorganization of ions on tube wall to form a co-axial cylinder structure with large diameter.^{2e,2f, 4a} Similar, the signal of semiconducting tube with larger diameter (centered at 148 cm^{-1}) disappeared, since the diameter of tube became larger after doping of ions of ILs in higher voltage, which is beyond the Raman response.

Meanwhile, the position of D band (1312-1323 cm^{-1}) downshifted after doping with EMI^+ (Fig.3d, 0- -2.5V), while it upshifted after doping with BF_4^- (Fig.3c, 0-2.5V). However, the position of G band (1590~1604 cm^{-1}) both upshifted by doping with EMI^+ and BF_4^- . Apparent, defective carbon of tube (associated to D band) had dangling negative bonds, which was saturated by interaction with EMI^+ , but not for BF_4^- . For G band, associated to the perfect graphitic carbon structure, was introduced into defects whether interacting with BF_4^- or EMI^+ . The position of 2D band (2611~2637 cm^{-1}) is also upshifted with the increase of applied potential (Fig.5e, 5f). Note that Raman shift of D band at 1.5 V in pure ILs is 5 cm^{-1} , far smaller than that (16 cm^{-1}) at 1.5 V in organic electrolyte with solvent of ACN.^{4a} Probably, the larger size of solvated ions in organic electrolyte contributed to the strong response of Raman.⁷ The result confirmed the change of Raman shift is electrolyte dependent and revealed the different capacitance effect on different electrolytes discussed above.

In addition, the doping of EMI^+ or BF_4^- ions also affected the intensity ratio of D band to G band (I_D/I_G) and the intensity ratio of 2D band to G band (I_{2D}/I_G). I_D/I_G value is increased drastically from 0.132 to 0.246 by doping BF_4^- (Fig.5c) or increased from 0.132 to 0.33 by doping of EMI^+ (Fig.5d) with the increased potential. I_{2D}/I_G values decreased drastically with the increase of applied potential, which enhanced the doping of EMI^+ and BF_4^- (Fig.5e, 5f). The results clearly suggested the enhanced interaction of EMI^+ or BF_4^- with tube wall at high potential. As to the state at 4V, theoretically, ions in larger amount will deposit on tube wall. It will further increase the diameter of co-axial tube-ILs structure, which had no RBM signal at 100-300 cm^{-1} .^{4c} Similar, the change trends of RBM peak, D band, G band and 2D band at 3-4 V to those at 1-2.5V could be expected. Note that, Raman signal recovered to that of pristine after the discharge, validating the stability of such charge mode. Otherwise, the decomposition of electrolyte produced amorphous carbon, resulting in the irreversible increase of I_D/I_G value.^{4a}

As follow, we studied the Raman response after the doping of EMI^+ or BF_4^- on the graphene (Fig.6). Similar trends were observed on the decreased peak intensity for D band, G band, 2D band after doping. But the peak position of them is less influenced with the increase of potential, compared to those of SWCNT. In addition, the change of I_D/I_G value is also insignificant compared to those of SWCNT, due to the pristine high defective degree of graphene (with higher pristine I_D/I_G value of 1.3), prepared by the chemical exfoliation method.

Such comparison validated the special electronic state of SWCNT (rolled up graphitic layer) play an important role in enhancing the interaction of ions,^{1h,2c} and, consequently, exhibited a better capacitance effect in new charge mode to achieve high energy density in high power density. Our study revealed the already-existed electrode had unexpected large potential in capacitance. New method or standard should be established to evaluate and understand their potential, depending not only on SSA, accessible SSA, but also on the configuration structure of electrode. It is very useful for the further fabrication of new electrode structure.

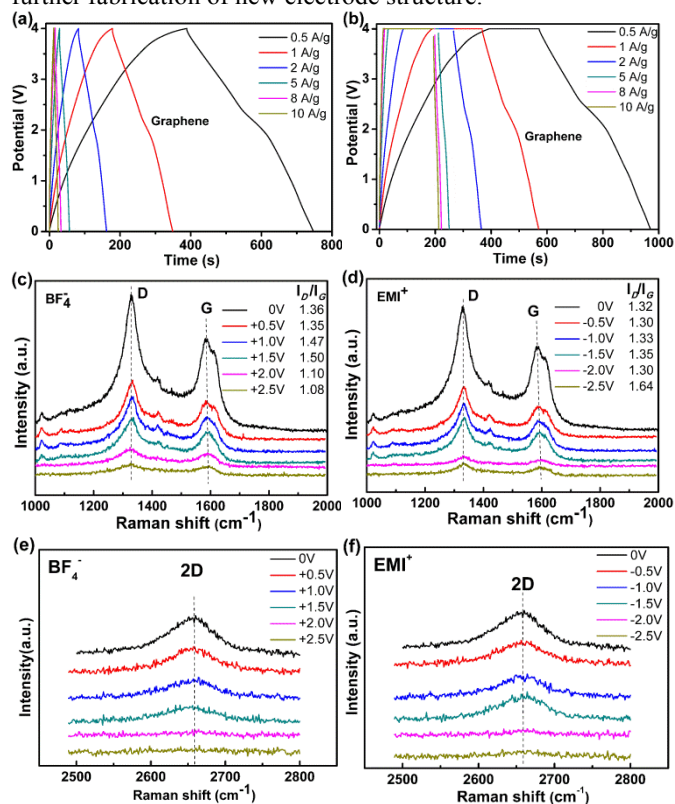


Fig.6 Different charge mode of graphene SCs at 4V: (a) Galvanostatic charge mode and (b) new charge mode; *In situ* Raman information of graphene in SC cell: D band and G band change of (c) BF_4^- doping and (d) EMI^+ doping; 2D band change of (e) BF_4^- doping and (f) EMI^+ doping.

Conclusions

We evidenced that the capacitance of SWCNT can approach to $16 \mu\text{F}/\text{cm}^2$ in wide range of current density. *In situ* Raman characterization validated that the enhanced doping of ions on tube wall with the increase of voltage. The comparison with a large size graphene highlights the advantage of configuration of SWCNT, which had small diameter and macropores in large amount accessible to ions easily. The charge mode used in the present work allowed 67 % increase of energy release at power density of 20 kW/kg. It provided a special application calling for high energy density under high power density, where the energy efficiency is not the first priority.

Acknowledgements

The authors thank the support of National 973 program of 2011CB932602, NSFC program of 21376135 and key program of 51236004.

Notes and references

Department of Chemical Engineering, Tsinghua University, Beijing 100084, PR China, E-mail: qianwz@tsinghua.edu.cn; Fax: +86 10 6277 2051; Tel: +86 10 6279 4133

Electronic Supplementary Information (ESI) available: [details of any supplementary information available should be included here]. See DOI: 10.1039/b000000x/

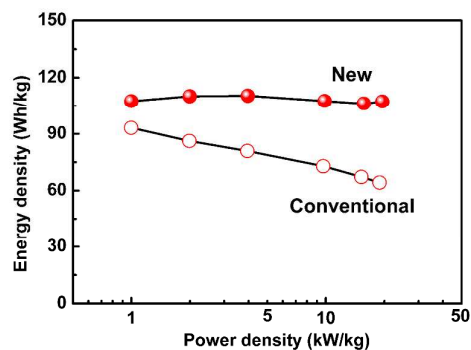
- (a) M. Inagaki, H. Konno, O. Tanaike, *J Power Sources*, 2010, **195**, 7880–7903. (b) A. S. Arico, P. Bruce, B. Scrosati, J. M. Tarascon, W. V. Schalkwijk, *Nat Mater*, 2005, **4**, 366–377. (c) A. Izadi-Najafabadi, S. Yasuda, K. Kobashi, T. Yamada, D.N. Futaba, H. Hatori, M. Yumura, S. Iijima, K. Hata, *Adv Mater*, 2010, **22**, E235-E241. (d) Z. Q. Niu, W. Y. Zhou, J. Chen, G. X. Feng, H. Li, W. J. Ma, J. Z. Li, H. B. Dong, R. Y. Yan, D. Zhao, S. S. Xie, *Energy Environ Sci*, 2011, **4**, 1440–1446. (e) T. Hiraoka, A. Izadi-Najafabadi, T. Yamada, D.N. Futaba, S. Yasuda, O. Tanaike, H. Hatori, M. Yumura, S. Iijima, K. Hata, *Adv Funct Mater*, 2010, **20**, 422–428. (f) A. Izadi-Najafabadi, D. N. Futaba, S. Iijima, K. Hata, *J Am Chem Soc*, 2010, **132**, 18017–18019. (g) C. Zheng, W. Z. Qian, Y. T. Yu, F. Wei, *Particuology*, 2013, **11**, 409–414. (h) A. Izadi-Najafabadi, T. Yamada, D. N. Futaba, H. Hatori, S. Iijima, K. Hata, *Electrochem Commun*, 2010, **12**, 1678–1681.
- (a) C. J. Cui, W. Z. Qian, Y. T. Yu, C. Y. Kong, B. Yu, L. Xiang, F. Wei, *J Am Chem Soc*, 2014, **136**, 2256–2259. (b) J. L. Xia, F. Chen, J. H. Li, N. Tao, *J. Nat Nanotechnol*, 2009, **4**, 505–509. (c) T. Fukushima, A. Kosaka, Y. Ishimura, T. Yamamoto, T. Takigawa, N. Ishii, T. Ada, *Science*, 2003, **300**, 2072–2074. (d) J. S. Huang, B. G. Sumpter, V. Meunier, G. Yushin, C. Portet, Y. Gogotsi, *J Mater Res*, 2010, **25**, 1525–1531. (e) M. Deschamps, E. Gilbert, P. Azais, E. Raymundo-Piero, M. R. Ammar, P. Simon, D. Massiot, F. Béguin, *Nat Mater*, 2013, **12**, 351–358. (f) Y. A. Lei, C. X. Xiong, L. J. Dong, H. Guo, X. H. Su, J. L. Yao, Y. J. You, D. M. Tian, X. M. Shang, *Small*, 2007, **3**, 1889–1893. (g) J. Vatamanu, O. Borodin, G. D. Smith, *J Am Chem Soc*, 2010, **132**, 14825–14833.
- (a) Q. Wen, W. Z. Qian, F. Wei, Y. Liu, G. Q. Ning, Q. Zhang, *Chem Mater*, 2007, **19**, 1226–1230. (b) C. Zheng, W. Z. Qian, C. J. Cui, Q. Zhang, Y. G. Jin, M. Q. Zhao, P. H. Tan, F. Wei, *Carbon*, 2012, **50**, 5167–5175. (c) S. Hummers, R. Offeman, *J Am Chem Soc*, 1958, **80**, 1339–1339. (d) Y. W. Zhu, S. Murali, M. D. Stoller, K. J. Ganesh, W. W. Cai, P. J. Ferreira, A. Pirkle, R. M. Wallace, K. A. Cychoz, M. Thommes, D. Su, E. A. Stach, R. S. Ruoff, *Science* 2011, **332**, 1537–1541. (e) C. Y. Kong, W. Z. Qian, C. Zheng, Y. T. Yu, C. J. Cui, F. Wei, *Chem Commun*, 2013, **49**, 10727–10729.
- (a) P. W. Ruch, L. J. Hardwick, M. Hahn, A. Foelske, R. Koetz, A. Wokaun, *Carbon*, 2009, **47**, 38–52. (b) L. Kavan, L. Dunsch, *Chem Phys Chem*, 2007, **8**, 974–998. (c) G. U. Sumanasekera, J. L. Allen, S. L. Fang, A. L. Loper, A. M. Rao, P. C. Eklund, *J Phys Chem B*, 1999, **103**, 4292–4297. (d) M. Stoll, P. M. Rafailov, W. Frenzel, C. Thomsen, *Chem Phys Lett*, 2003, **375**, 625–631. (e) P. M. Rafailov,

- M. Stoll, C. Thomsen, *J Phys Chem B*, 2004, **108**, 19241-19245.
- (f)A. Jorio, M. A. Pimenta, A. G. S. Filho, R. Saito, G. Dresselhaus, M. S. Dresselhaus, *New J Phys*, 2003, **5**, 139.1-139.17.
- 5 (a)S. M. Chen, K. Kobayashi, Y. Miyata, N. Imazu, T. Saito, R. Kitaura, H. Shinohara, *J Am Chem Soc*, 2009, **130**, 14850-14851. (b)S. M. Chen, G. Z. Wu, M. L. Sha, S. R. Huang, *J Am Chem Soc*, 2007, **129**, 2416-2417.
- 6 B. W. Ricketts, C. Ton-That, *J Power Sources*, 2000, **89**, 64-69.
- 7 (a)J. Chmiola, C. Largeot, P. L. Taberna, P. Simon, Y. Gogotsi, *Science*, 2010, **328**,480-483. (b) J. Chmiola, C. Largeot, P. L. Taberna, P. Simon, Y. Gogotsi, *Angew Chem. Int. Ed*, 2008, **47**, 3392-3395. (c)C. Merlet, B. Rotenberg, P. A. Madden, P. L. Taberna, P. Simon, Y. Gogotsi, M. Salanne, *Nat Mater*, 2012, **11**, 306-310.
- 8 (a)J. J. Yoo, K. Balakrishnan, J. S. Huang, V. Meunier, B. G. Sumpter, A. Srivastava, M. Conway, A. L. M. Reddy, J. Yu, R. Vajtai, P. M. Ajayan, *NanoLett*, 2011, **11**, 1423-1427. (b) N. Jha, P. Ramesh, E. Bekyarova, M. E. Itkis, R. C. Haddon, *Adv Energy Mater*, 2012, **2**, 438-444. (c) C. G. Liu, Z. N. Yu, D. Neff, A. Zhamu, B. Z. Jang, *Nano Lett*, 2010, **10**, 4863-4868. (d)X. W. Yang, C. Cheng, Y. F. Wang, L. Qiu, D. Li, *Science*, 2013, **341**, 534-537. (e)B. G. Choi, M. H. Yang, W. H. Hong, J. W. Choi, Y. S. Huh, *ACS Nano*, 2012, **6**, 4020-4028.

Table of contents

Full capacitance potential of SWCNT electrode in ionic liquids at 4V

Yuntao Yu, Chaojie Cui, Weizhong Qian*, Fei Wei



SWCNT electrode exhibited capacitance of $16 \mu\text{F}/\text{cm}^2$ and energy density of $107 \text{ Wh}/\text{kg}$ in wide power density range at 4V.